Adaptive motion model for a mobile robot

F. Westerhout (4293940), J.F.R.W. Kievits (4448693), T.F. Zondag (4326954), T.S.A.Sow (4322134)

***Abstract*—We propose an online adaptive model that can be used to model the motion of a skid-steered mobile robot on different terrains. A mathematical model is designed to model the wheel slip interaction and the resultant forces using the Dugoff tire model. The motion of the robot is subsequently modeled using Newtonian dynamics and connected to the wheel slip model. This joint dynamic model is implemented in MATLAB and Simulink. Real-world experiments with the mobile robot are performed to gather data. On-board sensors and an external Motion Capture System are used to obtain measurements. These measurements are used in combination with a parameter estimation method to obtain adapted parameters for the Simulink model. The adapted model is shown to be accurate for different surfaces for small amounts of pure longitudinal slip (e.g. $|\kappa| < 0.1$). Furthermore, alternative approaches are proposed for modeling forces at larger amounts of longitudinal slip and situations of combined slip, based on measurements from the performed experiments.**

I. INTRODUCTION

Skid-steered mobile robots are widely used in many different fields, such as exploration, waste management, defense, security, and household services. These wheeled mobile robots move by rotating the wheels on the left and right side of the robot body independently at different velocities. This allows the robot to drive and steer without a mechanical steering system. As a result, skid-steered robots only have a few moving parts which makes them very robust. These robots are therefore suitable for outdoor use in rough environment conditions. However, the over-constrained wheel-ground interaction for skid-steered vehicles causes the wheels to both skid and roll while rotating [1]. Due to these cumulative phenomena it is challenging to develop accurate dynamic models for these mobile robots [2].

The robot platform used for this project is the Jackal Unmanned Ground Vehicle from Clearpath Robotics, which uses a skid-steered driving mechanism and is operated with ROS. Currently the controller of the Jackal has no dynamic model that accounts for slip at the wheel-surface contact, which occurs when the robot is in motion. As a result, the robot is unable to follow commanded trajectories accurately. Obtaining an accurate dynamic model of the skid-steered robot with an incorporated slip model would be very useful in future control research and development. Modelling of the system dynamics of skid-steered robots has already been investigated in multiple research papers [3] [4]. However, for the Jackall UGV there is no accurate dynamical model present. Most of the research on online model identification with incorporated wheel slip is focused on larger vehicles, such as agricultural vehicles [5]. These research papers are not useful when regarding a skid-steered robot due to the large differences in the kinematics of these different types of vehicles. Therefore, the aim of this project is to build an accurate adaptive motion model, that accounts for non-linear slip behaviour, for a skid-steered mobile robot.

This paper is organized as follows. In Section II, the relevant background theory on the topic of dynamical modeling of wheeled mobile robots will be described as well as the preliminaries. This includes relevant information about the robot platform, analysis of the dynamics of the different subsystems and the wheel-ground interaction model. Section III describes the experimental setup, the measurement procedure and the processing of data. In Section IV, the results of the experiments will be presented. Section V discusses the obtained experimental results and compares these with model simulations. Finally, a conclusion is presented and recommendations are made for future research. [1]

II. BACKGROUND AND THEORY

A. Jackal mobile robot

The ROS-operated Jackal has an x86 PC running Ubuntu, paired with a 32-bit microcontroller unit (MCU) and an inertial measurement unit (IMU). The MCU handles ROS inputs and outputs, power supply monitoring, and motor control. It also receives data from the integrated IMU and transforms this into ROS outputs. The wheels are powered by two DC motors, one on each side of the vehicle [6]. Sturctural parameters of the Jackal can be found in Table IV in the Appendix. The current control system for the Jackal can be seen in Figure 1. The Jackal receives an input signal from a Bluetooth controller. This signal consists of a forward and a rotational velocity for the robot, denoted by v and $\dot{\psi}$ respectively. A differential drive controller is then used to transform v and $\dot{\psi}$ into setpoints for the angular velocities for the left and right wheels, denoted by ω_{L} and ω_{R} respectively. These values are converted to a pulse width modulation signal for the DC motors. The DC motors then apply a torque to the wheels using a geared transmission. This makes the wheels rotate at angular velocities, $\tilde{\omega}_{\mathrm{L}}$ and $\tilde{\omega}_{\mathrm{R}}$. These values are measured by the integrated wheel encoders and sent back to the differential drive controller. This controller then changes the output signal after comparing $\tilde{\omega}_{\mathrm{L}}$ to ω_{L} and $\tilde{\omega}_{\mathrm{R}}$ to ω_{R}. The measured wheel velocities are also used to localize the robot in space using an odometry estimator. The data from this estimator is then used, along with filtered acceleration data from the IMU, in an extended Kalman filter to produce a data set containing all position and velocity values.

[1] This research has been conducted as part of the Bachelor End Project for Mechanical Engineering students at the TU Delft in the third year of their Bachelor studies.

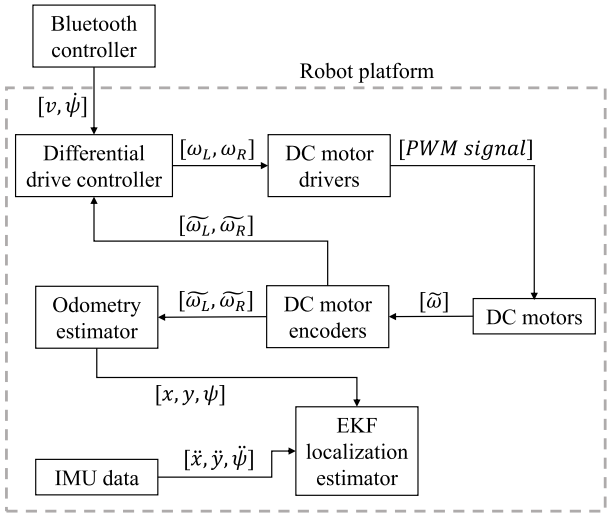

Fig. 1. Block diagram of the current Jackal control system

From the block diagram in Figure 1, the relevant subsystems of the Jackal can be identified. These subsystems are subsequently modeled using either algebraic or differential equations. This is described in the following paragraphs.

Assumptions are made to allow the modeling of the dynamics of the mobile robot without having to know certain parameters. These assumptions are listed below.

Modeling assumptions:

- The center of mass of the robot lies at the geometric center of the body frame.
- The normal forces are equally distributed among the four wheels when stationary and when in motion.
- The robot is driving on a flat surface and the wheels are always in contact with the ground.
- Friction forces are assumed to be constant.
- The motion model always starts from rest

B. Differential drive controller

In the differential drive controller the left and right wheel velocities are calculated independently. A simplified model of a skid-steered vehicle is used in these calculations. A kinematic diagram of this vehicle is shown in Figure 2.

The differential drive controller calculates the velocities as shown below:

$$\omega_{\mathrm{R}} = \frac{2v - \dot{\psi}W}{4r} \tag{1}$$

$$\omega_{\mathrm{L}} = \frac{2v + \dot{\psi}W}{4r} \tag{2}$$

where r and W denotes the radius of the wheels and vehicle width respectively; v and $\dot{\psi}$ are the linear input velocity and rotational input velocity of the Jackal respectively. The calculated angular velocities for the wheels are then converted into an analog voltage signal which is sent to the respective DC motors.

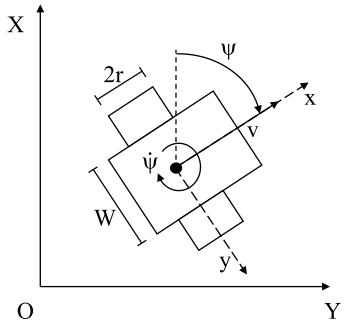

Fig. 2. Kinematic diagram of the vehicle as used in the differential drive controller

C. DC Motor

The motor equations give the torque T_m on the rotor in terms of the armature current i_{a} which is induced by the analog voltage signal.

$$T = K_{\mathrm{t}} i_{\mathrm{a}} \tag{3}$$

By using Newton's laws the following equation is obtained:

$$J_m \ddot{\theta}_{\mathrm{m}} + \left(b + \frac{K_t}{R_a} \right) \dot{\theta}_{\mathrm{m}} = T_m \tag{4}$$

where R_{a} denotes the armature resistance [7], J_{m} denotes the rotor inertia, b the viscous friction coefficient and K_{t} the torque constant.

D. Wheel dynamics

The assumptions mentioned before, allow the Jackal to be modeled as a combination of four separate wheels with the same wheel dynamics. The Jackal is therefore modeled using a quarter-car model. The forces acting on the wheel, as shown in Figure 3, are analyzed in the body fixed frame.

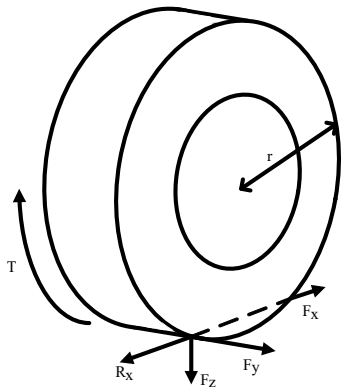

Fig. 3. Free-body diagram of the wheel with radius r: The torque T is giving a forward force F_x. The rolling resistance, lateral and normal force are denoted by R_x, F_y and F_z respectively. The arrows indicate the positive directions.

To calculate the torque applied to the wheel the following equation is used:

$$T_{\text{wheel}} = \frac{j\eta T_m}{2} \tag{5}$$

Here j is the ratio of the gear transmission between the DC motor and the wheels, η is the efficiency of this gear transmission and T_m is the total torque exerted by the DC motor. The angular acceleration of the wheels can then be found through the following equilibrium:

$$J_{\text{wheel}}\dot{\omega}_{\text{wheel}} = T_{\text{wheel}} - F_{x,\text{wheel}}r - R_{x,\text{wheel}}r \tag{6}$$

The direction of movement is in the x-direction. F_x represents the driving force of a wheel and R_x represents the rolling resistance force. The radius of the wheel is denoted r.

Furthermore, F_x is dependent on the amount of slip that occurs at the contact point of the wheel with the ground. To account for this slip, two semi-empirical estimation models have been considered, the Pacejka model [8] and the Dugoff model [9]. Both models express the linear traction force and the lateral force using the longitudinal slip κ and the slip angle α,

$$\kappa = \frac{\omega_{\text{wheel}}r - v_x}{\mid v_x \mid} \tag{7}$$

$$\alpha = \arctan\left(\frac{v_y}{\mid v_x \mid}\right) \tag{8}$$

Where v_x and v_y denote the velocity of the wheel hub in longitudinal direction and lateral direction respectively.

1) Pacejka Model: The standard form of the Pacejka model is given by,

$$P(q) = D{\cdot}sin[C{\cdot}\arctan\{Bq - E(Bq - \arctan(Bq))\}] \tag{9}$$

where B, C, D and E represent fitting constants characterized by stiffness, shape, peak and curvature of the fitting function respectively; the function $P(q)$ represent the forces on the tires based on:

- Vertical load per wheel F_z
- Wheel slip κ
- Slip angle α

Rewriting 9 to calculate the longitudinal force F_x and lateral force F_y gives

$$F_x(\kappa) = F_z D sin(C \arctan \{B\kappa - E[B\kappa - \arctan(B\kappa)]\}) \tag{10}$$

$$F_y(\alpha) = F_z D sin(C \arctan \{B\tan(\alpha) - E[B\tan(\alpha) - \arctan(B\tan(\alpha))]\}) \tag{11}$$

This formula is completed by using experimental data to estimate the B, C, D and E fitting constants. These are dependent on certain physical parameters of the wheel and surface [10]. Using the Pacejka model for online adaption is not ideal, when regarding simplicity and computational load, due to the relatively large number of parameters. If the number of parameters in the model would be smaller, the computation time needed for parameter estimation would also decrease. Therefore another model is considered with less parameters that have to be estimated.

2) Dugoff Model: A simplified form of the Dugoff model with longitudinal force F_x and lateral force F_y is given by

$$F_x(\kappa, f) = \frac{K_{x\kappa}\kappa}{1-\kappa} f(\lambda) \tag{12}$$

$$F_y(\alpha, \kappa, f) = \frac{K_{y\alpha}\tan\alpha}{1-\kappa} f(\lambda) \tag{13}$$

with a shape function to accommodate for the non-linear slip behaviour,

$$f(\lambda) = \begin{cases} \lambda(2-\lambda), & \text{if } \lambda < 1 \\ 1, & \text{if } \lambda > 1 \end{cases} \tag{14}$$

and a weighting coefficient,

$$\lambda(\kappa, \alpha) = \frac{\mu F_z(1-\kappa)}{2\sqrt{(K_{x\kappa}\kappa)^2 + (K_{y\alpha}\tan\alpha)^2}} \tag{15}$$

Here the friction coefficient μ is considered to be constant instead of a function of v, κ and α, as is normally the case [9]. This assumption can be made because the Jackal does not drive at high velocities like, for instance, cars do. The acceleration of the Jackal is also limited and therefore the values of the slip coefficient κ will be limited. This simplification implies that the model will be less accurate for large velocities or large values of κ but that is acceptable for the scope of this project. This simplification allows the model to be tuned with only three parameters, $K_{y\alpha}$, $K_{x\kappa}$ and μ. Here, both of the K-values are used to describe the physical stiffness of the tires and μ is used to describe the roughness of the surface. Ideally, the goal is to adjust only one parameter to allow the model to behave accurately on different surfaces. To achieve this goal the Dugoff model is preferred over the Pacejka model because of the smaller number of parameters that have to be estimated.

E. Vehicle dynamics

The 'xyz' frame in Figure 4 represents the body fixed frame of the Jackal. The x and y-axis coincide with the orientation of the vehicle in the longitudinal and lateral direction respectively. The z-axis is directed downward, perpendicular to the x and y-axis. The rotational motion along the x, y and z-axis are called roll, pitch and yaw respectively; denoted by β, ϕ and ψ respectively. However due to the fact that only planar motion is considered, both β and ϕ will always equal zero.

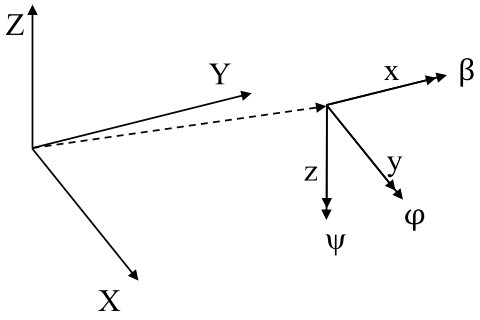

Fig. 4. Global and body fixed coordinate system, denoted by the axis 'XYZ' and 'xyz' respectively

The global coordinate system is represented by an 'XYZ' frame which is fixed to the ground. The motion of the Jackal happens relative to this frame. By using Newtonian dynamics, it is possible to describe the motion of the Jackal in terms of the forces applied to the vehicle.

An overview of all the relevant forces acting on the Jackal is given in Figure 5. Parameters l_1 and l_2 represent the respective distances from the wheel to the center of mass, denoted by symbol A, in x-direction; W represents the width of the vehicle. Each wheel is numbered from 1 to 4.

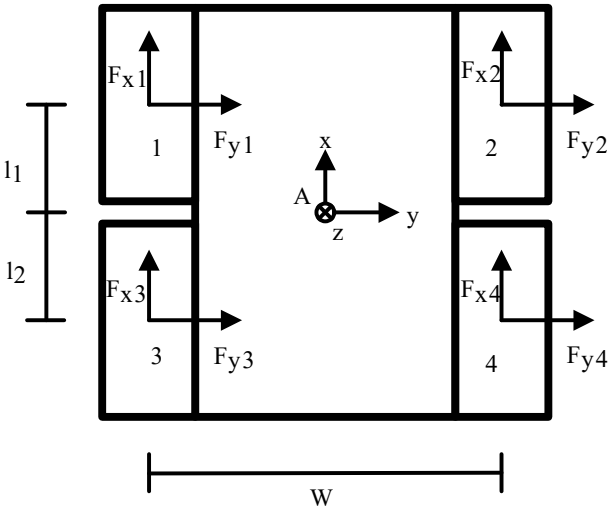

Fig. 5. Free-body diagram of the Jackal

Because the vehicle moves on flat ground, the motion in the z-axis is not taken into consideration. This results in the following equations of motion of the rigid body in the body fixed frame,

$$\sum F_x = m \cdot a_x \tag{16}$$

$$\sum F_y = m \cdot a_y \tag{17}$$

$$\sum M = I_{zz} \cdot \ddot{\psi} \tag{18}$$

Where the sums of the forces and moments are given by,

$$\sum F_x = F_{x1}+F_{x2}+F_{x3}+F_{x4}-R_{x1}-R_{x2}-R_{x3}-R_{x4} \tag{19}$$

$$\sum F_y = F_{y1}+F_{y2}+F_{y3}+F_{y4}-R_{y1}-R_{y2}-R_{y3}-R_{y4} \tag{20}$$

$$\begin{aligned}\sum M_A = {} & l_1(F_{y1}+F_{y2}-R_{y1}-R_{y2}) \\ & - l_2(F_{y3}+F_{y4}-R_{y3}-R_{y4}) \\ & + \frac{W}{2}(F_{x1}+F_{x3}-R_{x1}-R_{x3}) \\ & - \frac{W}{2}((F_{x2}+F_{x4}-R_{x2}-R_{x4})\end{aligned} \tag{21}$$

If the model is always assumed to start from rest, the following equations hold,

$$\int a_x \mathrm{d}t = v_x \tag{22}$$

$$\int a_y \mathrm{d}t = v_y \tag{23}$$

$$\int \ddot{\psi} \mathrm{d}t = \dot{\psi} \tag{24}$$

$$\int \dot{\omega}_{\text{wheel}} \mathrm{d}t = \omega_{\text{wheel}} \tag{25}$$

The values for v_x and v_y are then used for calculations of κ and α in the next iteration of the model. The values can be compared with the input data as described in Section III.

III. Method

The method of the research can be divided into several steps. The dynamic behaviour of the Jackal is firstly described in a mathematical model, which is then converted to Simulink and MATLAB. Then a wide range of experiments is conducted on two different types of terrain. This data is subsequently used for estimating parameters of the model.

The experiments with the mobile robot are performed in a lab where it is possible to track the robot externally using a motion capture system. This way, the motion model can be compared to this external reference, which is regarded as ground truth data. The experiments are carried out on two different surfaces; smooth lino and rough carpet. The simulation results are compared to the ground truth data of an experiment on the first surface type. From this comparison, a set of optimized parameters for the dynamic model can be obtained for that first surface type. The output of the model is then compared to the ground truth data for the same experiment on the other surface type. By comparing simulation results with the data again, a new set of optimized parameters is obtained for the second surface.

A. Experimental setup

The experiments have been performed in the Delft Center for Systems and Control lab. To accurately measure the position of the Jackal, a Motion Capture System by Optitrack is used. A schematic overview of the experimental setup can be seen in Figure 6.

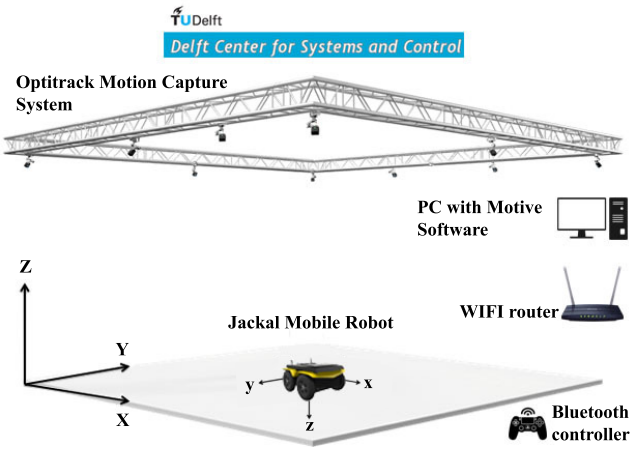

Fig. 6. Experimental setup of external Motion Capture System

This system uses 10 high-tech infrared cameras that are able to capture movements within a millimeter accuracy at a rate of 120 Hz [11]. Besides this external measuring system, measurements of internal sensors of the Jackal are also logged simultaneously. This data is transmitted using WiFi to a nearby computer. Here the measured data is stored in a format called ROS bags. These ROS bags can be read using MATLAB and graphical representations can be plotted.

A brief description of the experiments is shown in Table I. Experiment 1 gives data about the longitudinal wheel slip of the vehicle at constant speed. Experiment 2 is conducted to find data about longitudinal slip during acceleration and deceleration. To find data about lateral slip, experiments 3-8 are conducted. The combination of these experiments generates enough data to develop a full overview on the Jackal's dynamics. Each experiment is conducted multiple times to minimize measurement errors.

TABLE I
OVERVIEW OF EXECUTED EXPERIMENTS

Experiment	Description
1	Straight line, with $v = 0.4\mathrm{m/s}$
2	Straight line, accelerating from rest with $a = 1.0\mathrm{m/s^2}$
3	U-shape, with $v = 0.4\mathrm{m/s}$, turning left
4	U-shape, with $v = 0.4\mathrm{m/s}$, turning right
5	Paperclip oval shape, with $v = 0.4\mathrm{m/s}$ in corners and $a = 1.0\mathrm{m/s^2}$ in straights
6	Square shape, with $v = 0.4\mathrm{m/s}$ in linear direction and rotating at position in corners
7	3 consecutive circles, with $v = 0.4\mathrm{m/s}$, counter-clockwise
8	3 consecutive circles, with $v = 0.4\mathrm{m/s}$, clockwise

B. Parameter estimation

The estimation of unknown model parameters is done using the Parameter Estimation Tool in Simulink. This tool uses a batch of measured input and output data from the Jackal in combination with a cost function to determine the optimal parameters. In this case the ordinary least squares method is used to estimate the parameters. This method, like most linear estimators, works well for input values with high reliability and consistency [12]. The ordinary least squares method might deviate and become unreliable if the input variable is not consistent. However, it has been proven that this method works well for estimating dynamic robot model parameters for online applications [13]. This is the reason that the ordinary least squares method is used to estimate unknown model parameters numerically.

The unknown parameters that are estimated using the estimation tool are,

Jackal parameters:

- b, the viscous friction coefficient of the DC motors.
- J_m, the rotor and gear head inertia of the DC motors.

Dugoff model parameters:

- μ, the friction coefficient in the Dugoff model
- $K_{y\alpha}$, the cornering stiffness of the tire
- $K_{x\kappa}$, the longitudinal slip stiffness of the tire

The DC motors are not used in estimating the Dugoff parameters from the experimental data. This is mainly because the angular velocity of the wheels is measured directly. These measurements would therefore be a more accurate input for the Dugoff model than simulated wheel velocities. Since parameter estimation methods for DC motors are fairly well-known [14], it is not expected that the estimated motor parameters will have a large impact on the overall model. However, when simulation results from the DC motors are used as inputs for the Dugoff model this impact might accumulate. Therefore the choice was made to only use the measured wheel velocity from the wheel encoders.

C. Online adaptation

The goal of online adaptation is to collect the measured data from the Jackal and use this to adapt parameters in the motion model. To achieve this the data is stored in batches of a certain size. These batches can then be used in combination with a numerical estimation method as mentioned before. The parameter values found by this process are then used to update the relevant parameters in the motion model. The only value that has to be estimated for terrain adaptation is μ. The estimation process has to be executed in a relatively short period of time, because otherwise the model cannot be considered as online adaptive. This limits the complexity of the model and the estimation method due to computation time. Therefore simpler models with less parameters are preferred as mentioned in Section II.

D. Experimentation on different surfaces

The set of experiments presented in table I is conducted on two different surfaces. The experiments are first performed on a smooth lino floor and then the same set of experiments is conducted on rough carpet as mentioned before. The goal of

experimenting on different surfaces is to let the model estimate a new value for μ, the friction coefficient in the Dugoff model.

This value is estimated by fitting a Dugoff curve to measured data, particularly the linear traction force F_x, the lateral skid force F_y and their relation to the slip coefficient κ and the slip angle α respectively. Graphical representations of the Dugoff model with different parameters are shown in Figure 7 and Figure 8.

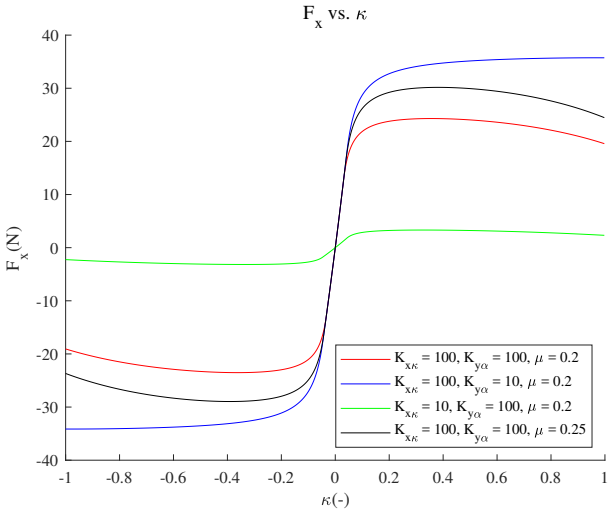

Fig. 7. Linear traction force F_x using Dugoff model vs slip coefficient κ for different values of $K_{x\kappa}$, $K_{y\alpha}$ and μ.

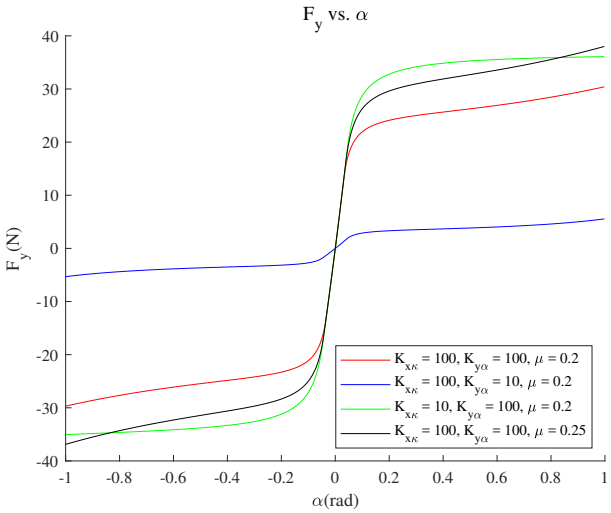

Fig. 8. Lateral skid force F_y using Dugoff model vs slip angle α for different values of $K_{x\kappa}$, $K_{y\alpha}$ and μ.

It is clear that the simplified Dugoff model is linear for small values of the slip coefficient or slip angle. Non-linear behaviour is displayed for larger values of these variables. It is expected that the measurements from the experiments show similar behaviour. This will allow the Dugoff model to be applied by changing the model parameters. The aforementioned method of the least squares error is able to estimate these parameters, if provided with smooth data without discontinuities as mentioned before.

IV. Results

In this section the MATLAB/Simulink model is presented and results of selected performed experiments are displayed.

Figure 9 shows a schematic overview of the designed Simulink model. The Simulink model uses the commanded linear and rotational velocity as input for the Jackal. The commanded linear and rotational velocity are converted to the angular velocities of the wheels according to equations 1 and 2. A pulse width modulation signal is then sent to the DC motors to adjust the torque accordingly. The torque from the DC motors is derived from equations 4 and 5. The torques are subsequently the input for the individual wheels. From the wheels, the rotational velocity ω_i is measured and used as input for the Dugoff model. The forces are then calculated using equations 12, 13, 14 and 15; These are then supplied to the rigid body from which the equations of motion 16, 17 and 18 for the vehicle can be derived. Integrating the equations of motion using equations 22, 23 and 24 gives the velocity components and heading rate of the Jackal. These outputs are then fed back into the Duggoff model to estimate the model parameters κ and α using equations 7 and 8.

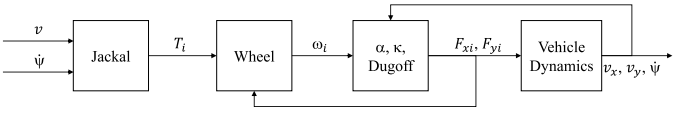

Fig. 9. Schemematic representation of the Simulink model

A. Measured quantities

All incoming data signals are filtered to reduce the amount of noise in the measured signals. A low-pass Butterworth filter is used because this filter works well without delaying the signal significantly [15]. The signals are plotted for experiment 1 and 4 on lino and experiment 1 on carpet in Appendix D. The characteristics of the measured signals are listed below in Table II.

TABLE II
Overview measured signals

System	Sample rate(Hz)	Description	Symbol (Unit)
IMU	70	Acceleration in local x-direction	$a_x(\mathrm{m/s^2})$
		Acceleration in local y-direction	$a_y(\mathrm{m/s^2})$
MOCAP	120	Global X position	X(m)
		Global Y position	Y(m)
		Yaw angle of the vehicle	ψ(rad)
Wheel encoder	20	Angular velocity left wheels	ω_L (rad/s)
		Angular velocity right wheels	ω_R (rad/s)
Bluetooth controller	20	Commanded linear velocity	v(m/s)
		Commanded angular velocity	$\dot{\psi}$(rad/s)

The wheel encoders measure the angular wheel velocity of the left and right wheels separately. Because the two wheels on each side are connected to one motor the angular velocity of

the wheels on the same side remains equal. The signal from the encoders is plotted in Figure 10, Figure 19 and Figure 28.

For the plots with respect to the orientation of the Jackal in space, data from the MOCAP system is used. The 2D position of the center of the robot body is shown in Figure 12, 21 and 30 The yaw angle is shown graphically in Figure 13, 22 and 31. Also the position in X and Y-direction is differentiated over time to obtain the velocity of the Jackal in Cartesian coordinates. These are then combined with the derivative of the yaw angle and the yaw angle itself to obtain the velocity in the local frame. This linear velocity is shown in Figure 14, Figure 23 and Figure 32.

The accelerations measured by the IMU are used to calculate the forces that are exerted on the body. The measured accelerations are linearly dependent on the resultant force on the body. However for simplification, the friction forces are not considered. The resultant force is calculated using Newton's second law:

$$\sum F = m \cdot a \tag{26}$$

The force in x-direction is plotted against time in Figure 15, 24 and 33. The longitudinal traction forces are also plotted against the respective measured values of the slip coefficient κ (-). This allows the application of a Dugoff model to the data. This can be seen in Figure 16, Figure 25 and Figure 34.

For experiment 1, a Dugoff model was selected that best matched the measured data. No statistical approach is used because of the large number of outliers in the data which provide unreliable results when combined with a numerical parameter estimation method. Instead the parameters of the Dugoff model were optimized to ensure that it crosses the highest number of data points possible. The model was only accurate for small values of κ, (e.g. $|\kappa| < 0.1$) as can be seen in Figure 16 and Figure 34. The estimated parameters are listed in Table III.

This experiment is repeated in exactly the same way on a rough carpet surface. The measured forces are shown in Figure 34 and Figure 36. As can be seen, both experiments seem to fit well with the Dugoff model. However, in these experiments only longitudinal slip is considered. It is possible to neglect the forces in the local y-direction due to the small values of F_y in both experiments. This is shown, when comparing Figure 17 and Figure 35 with Figure 15 and Figure 33 respectively, as the peak values of F_x are over ten times larger than F_y. Furthermore there also does not seem to be a clear relation between α and F_y, as shown in Figure 36.

As expected, a higher value of μ matches the data better in the experiment with the rough carpet, with respect to the same experiment on the lino surface. This value is $\mu = 0.20$.

An overview of the parameter values is given below in Table III.

When Figure 25 and Figure 27 of experiment 4 are considered, it is clear from the shown data that an inconsistency occurs in the measured forces. In these figures the force seems to have two components which behave very differently from each other. One component seems to behave according to the Dugoff model but there is also one value that seems to follow a different curve. Due to these unexpected inconsistencies the choice was made to not compare the measured values with the Dugoff model. The model parameters of the Dugoff model also varied too much within the data sets to find the cause of the inconsistencies or apply a numerical parameter estimation method.

TABLE III
ESTIMATED PARAMETER VALUES FOR $K_{y\alpha}$, $K_{x\kappa}$ AND μ

Floor type	$K_{y\alpha}$ (N/rad)	$K_{x\kappa}$ (N/rad)	μ (-)
Lino Exp. 1	72	70	0.18
Carpet Exp. 1	72	70	0.20

V. DISCUSSION

In this section the aforementioned results will be discussed. It is clear from the experiment plots that the Dugoff model is not well suited to model the combined slip of the Jackal. Because of the fact that the model is simplified, the complete characteristics from the traction or lateral force, with respect to the slip coefficient or the slip angle respectively, cannot be approximated to a high degree. This leads to differences when comparing the outcome of the Dugoff model with the measured forces and accelerations as can be seen in the figures. However, in simple experiments, where only pure longitudinal slip is considered, the slip model is able to approximate the measured data quite closely for small values of κ and α. For larger values, the Pacejka model is recommended due to the ability to model the force curve with more accuracy. However, this might have negative effects on computation time and model simplicity.

With the measured data the parameters of the Dugoff model have to be optimized. The initial goal was to use batches of input and output data in combination with a discrete numerical estimation method. However, this advanced form of estimation is not well suited for data with a lot of noise or inconsistencies [12]. For a numerical estimation method to work well, the outliers of the data would have to be removed manually which involves data manipulation. The dynamic model with the estimated parameters would therefore be relatively unreliable.

The choice was made to estimate values for μ, $K_{y\alpha}$ and $K_{x\kappa}$ by only using the acceleration data that matched our expectation of what the forces should be. The curves with these expected forces are found in Figure 7 and 8. As mentioned earlier, friction forces are neglected in this approximation. The Dugoff model therefore models a traction force for positive slip variables and a breaking force for negative slip variables. Even though this might not be entirely the case in reality, it allows for simpler model approximation and parameter estimation which is acceptable for the scope of this research.

As mentioned earlier, the traction force and lateral force show large inconsistencies with the Dugoff model in experiment 4.

This might be due to the shape of the trajectory in which the Jackal is subjected to both lateral and linear slip. It is likely that the simplified Dugoff model is not well suited for combined slip and a weight function should be used to counter this problem [9].

There are also other reasons, which are applicable to all experiments, why the data does not seem to fit well to the Dugoff model.

Firstly, because the data is retrieved from real world experiments, it is subjected to noise and disturbances from the environment. At low velocities, this leads to high values for the slip coefficient and slip angle. This results in data outliers when comparing the data of the slip coefficient to the measured linear traction force for example. Either sensors with a higher sensitivity should be used or the experiments should be performed at higher velocities.

Secondly, the sensors that were used during the experiment do not measure the needed quantities for calculation directly. Instead algebraic equations along with differentiation or integration have to be used to obtain the needed values. This always leads to irregularities of the obtained data with respect to the real value. An example of this behaviour can be seen in Figure 19. An error analysis of all the incoming signals could be used to quantify the induced irregularities in the measured data. This unfortunately does not fit within the scope of this research.

Thirdly, the signals from the sensors are not very reliable. The sensors do not measure the different quantities at constant sample rates and often show an offset in the measured signal. Both the Motion Capture System and the inertial measurement unit in the Jackal show areas, where sampling is not performed or is performed at a different rate, within the data sequence. This provides synchronization problems when comparing these values with each other. Re-sampling the faulty data sets solves these problems somewhat. It is also recommended that the sensors are re-calibrated to ensure a minimal offset in the measured signal.

Lastly, the real value of μ is dependent on multiple environment variables such as temperature, wheel pressure and the surface roughness [9] [16]. The fact that this value is simplified, to allow parameter estimation to be performed without knowing the environment variables, can lead to an overly simplified expression for the Dugoff model. For example, the wheel pressure of the wheels of the Jackal is found not to be consistent. This could highly influence the value of μ.

VI. Conclusion and recommendations

The goal of this research paper is to develop an adaptive motion model for a skid-steered mobile robot that could be used for different terrains. As mentioned before, such a model would be useful in further research with regard to controller design for these robots. However the dynamic model should satisfy a certain degree of accuracy. The model that is presented in this paper does not yet satisfy this degree of accuracy. Due to large errors and inconsistencies in the measured data, it is difficult to establish any statistical proof of concept of the model. However, from the obtained data it is clear that the Dugoff slip model can be used to simulate the wheel-ground dynamics of the Jackal for small values of pure longitudinal slip (e.g. $|\kappa| < 0.1$). For high values of pure slip or combined slip, a more advanced version of the Dugoff model is proposed.

Another slip model is also proposed, the Pacejka model, which works better for high values of pure slip or combined slip as well. This model would therefore match the data better but advanced numerical parameter estimation techniques would have to be used to obtain the large number of variables necessary for this Pacejka model.

For further research it is essential to limit irregularities in the measured data. This can be achieved through experimenting with higher velocities resulting in a smaller fraction of noise in the signal. These actions also involve recalibrating all of the used sensors and perhaps even using sensors with a higher sensitivity. This prevents excessive filtering and manipulation of the measured data and allows the model itself to be applied with more certainty.

Acknowledgements

The authors would like to thank their supervisors Prof. dr. R. Babuska, dr. J. Alonso Mora and ir. Boaz Floor for their valuable knowledge and advice. The authors would also like to thank dr. B. Shyrokau for his help on the Pacejka and Dugoff tire model.

References

[1] O. Chuy, E. G. Collins, W. Yu, and C. Ordonez, "Power modeling of a skid steered wheeled robotic ground vehicle," in *2009 IEEE International Conference on Robotics and Automation*. IEEE, 2009, pp. 4118–4123.

[2] J. Yi, D. Song, J. Zhang, and Z. Goodwin, "Adaptive trajectory tracking control of skid-steered mobile robots," in *Robotics and Automation, 2007 IEEE International Conference on*. IEEE, 2007, pp. 2605–2610.

[3] D. A. Krishnamurthy, "Modeling and simulation of skid steered robot pioneer 3at," 2008.

[4] I. D. J. IGUARAN SUAREZ and O. E. DÍAZ POMPA, "Control of in-wheel motors for an outdoor skid-steering robot," 2016.

[5] F. Rogers-Marcovitz and A. Kelly, "On-line mobile robot model identification using integrated perturbative dynamics," in *Experimental Robotics*. Springer, 2014, pp. 417–431.

[6] "Jackal ugv - small weatherproof robot - clearpath," last required on 2018-01-06. [Online]. Available: https://www.clearpathrobotics.com/jackal-small-unmanned-ground-vehicle/#tech-specs

[7] G. F. Franklin, J. D. Powell, and A. Emami-Naeini, *Feedback control of dynamic systems*, 7th ed. Pearson Education Limited, 2015.

[8] E. Bakker, L. Nyborg, and H. B. Pacejka, "Tyre modelling for use in vehicle dynamics studies," *SAE Transactions*, pp. 190–204, 1987.

[9] J. van Ginkel, "Estimating the tire-road friction coefficient based on tire force measurements," Master's thesis, Delft University of Technology, 2014.

[10] "Tire (friction parameterized)," last required on 2018-01-06. [Online]. Available: https://nl.mathworks.com/help/physmod/sdl/ref/tireroadinteractionmagicformula.html

[11] "Network Embedded Robotics Lab," http://spaceinstitute.tudelft.nl/research/, [Online; accessed 2019-01-07].

[12] B. B. Richard Aster and C. Thurber, *Classification of parameter estimation and inverse problems*, 2018, vol. 3.

[13] H. S. Karl Iagnemma, Shinwoo Kang and S. Dubowsky, "Online terrain parameter estimation for wheeled mobile robots with application to planetary rovers," 2004.

[14] "Estimating dc motor parameters," last required on 2018-01-06. [Online]. Available: https://nl.mathworks.com/videos/estimating-dc-motor-parameters-97057.html

[15] A. S. W. Alan V. Oppenheim, *Signals and Systems*, 2013, vol. 2.

[16] M. U. S. Muller and K. Hedrick, "Estimation of the maximum tire-road friction coefficient," *Journal of Dynamic Systems, Measurement, and Control*, vol. 125, pp. 607–617, 2004.

APPENDICES

Appendix A - Nomenclature

symbol	Description
a	acceleration in meter per second squared
α	slip angle
b	viscous friction coefficient in newton meter second
β	angle around the x-axis in radian
η	gearhead efficiency
e	back EMF voltage in volt
F_x	longitudinal force in newton
F_y	lateral force in newton
F_z	normal force in newton
i_{a}	armature current in ampere
I_{zz}	moment of inertia of the Jackal in the z-direction
J_{m}	rotor and gear head inertia of the DC motors in kilogram per meter squared
j	DC motor gear head ratio
K_{t}	torque constant
K_{e}	electric constant
κ	wheel slip
$K_{x\kappa}$	longitudinal slip stiffness
$K_{y\alpha}$	cornering stiffness
l_1	distance of front axis to the center of gravity A in meter
l_2	distance of rear axis to the center of gravity A in meter
λ	weighting coefficient
m	vehicle mass in kilogram
M	moment force in newton meter
ω_{L}	rotational velocity of left wheel in radian per second
ω_{R}	rotational velocity of left wheel in radian per second
ϕ	angle around the y-axis in radian
ψ	angle around the z-axis in radian
$\dot{\psi}$	angular velocity around the z-axis in radian per second
$\ddot{\psi}$	angular acceleration around the z-axis in radian per second squared
r	radius of the wheels in meter
R	friction force in newton
R_{a}	armature resistance in ohm
T	torque in newton per meter
$\dot{\theta}_{\mathrm{m}}$	rotational velocity of DC motor rotor shaft in radian per second
$\ddot{\theta}_{\mathrm{m}}$	rotational acceleration of DC motor rotor shaft in radian per second squared
U_{a}	armature voltage in volt
v	body-fixed forward velocity in meter per second
v_x	longitudinal velocity in meter per second
v_y	lateral velocity in meter per second
W	vehicle width in meter
x	body-fixed position in the x-direction in meter
X	global X coordinate
y	body-fixed position in the y-direction in meter
Y	global Y coordinate
z	body-fixed position in the z-direction in meter
Z	global Z coordinate

Appendix B - Experiment plots

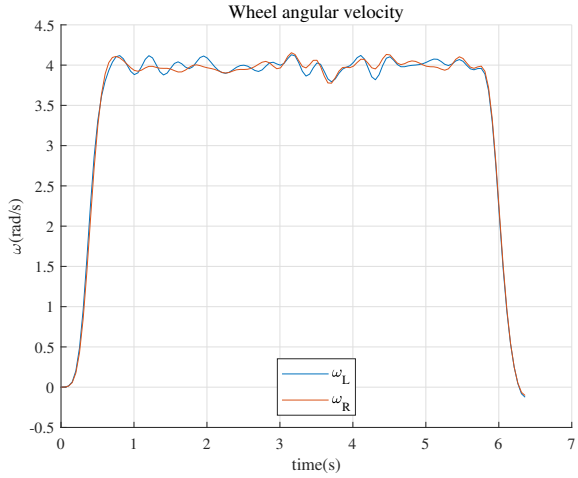

Fig. 10. Experiment 1 (Lino): Graphical representation of the angular velocities of the left- and right side wheels.

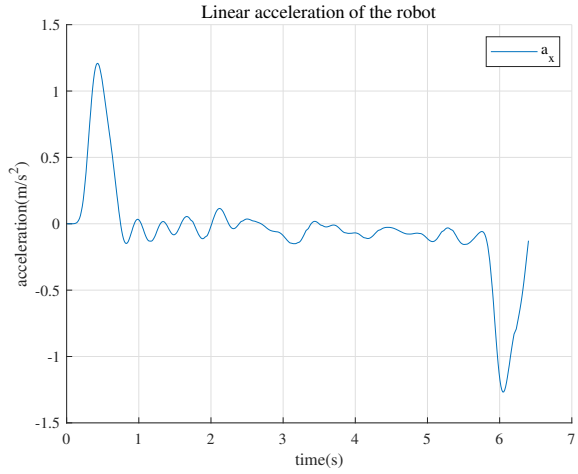

Fig. 11. Experiment 1 (Lino): Graphical representation of the linear acceleration of the Jackal robot.

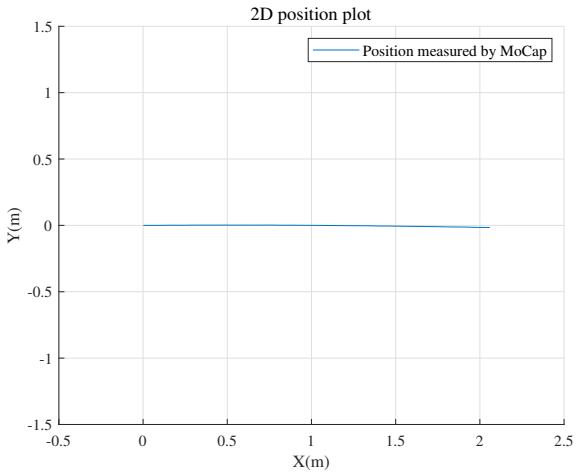

Fig. 12. Experiment 1 (Lino): Graphical representation of the 2D trajectory of the Jackal robot starting at (0,0).

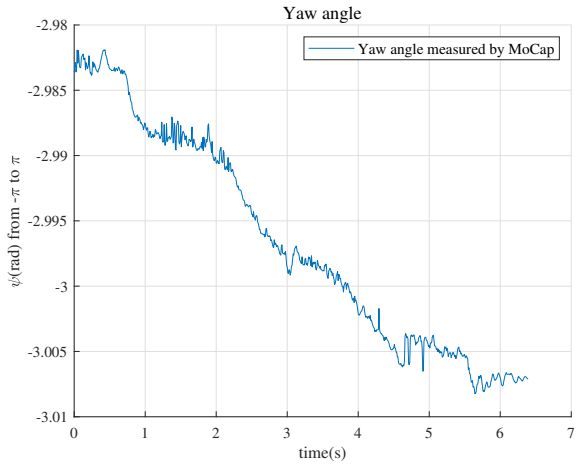

Fig. 13. Experiment 1 (Lino): Graphical representation of the yaw angle of the Jackal with respect to the global frame.

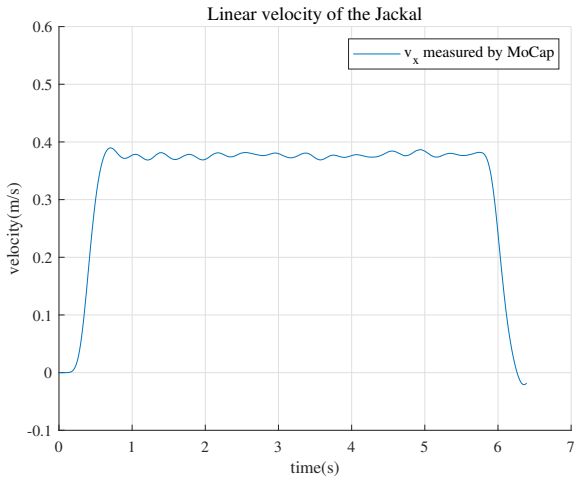

Fig. 14. Experiment 1 (Lino): Graphical representation of the linear velocity of the Jackal in the local frame.

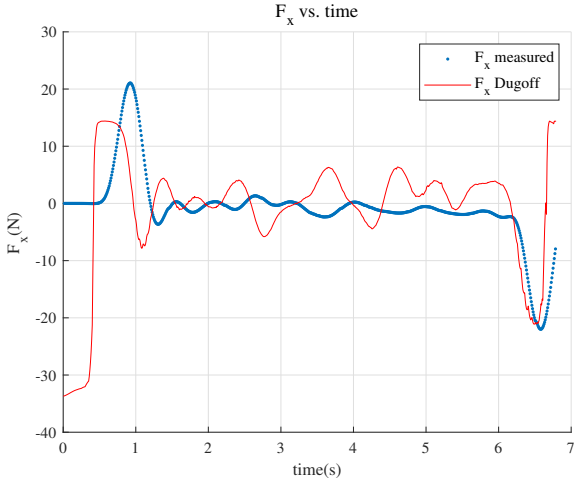

Fig. 15. Experiment 1(Lino): measured longitudinal traction force F_x vs time with Dugoff model.

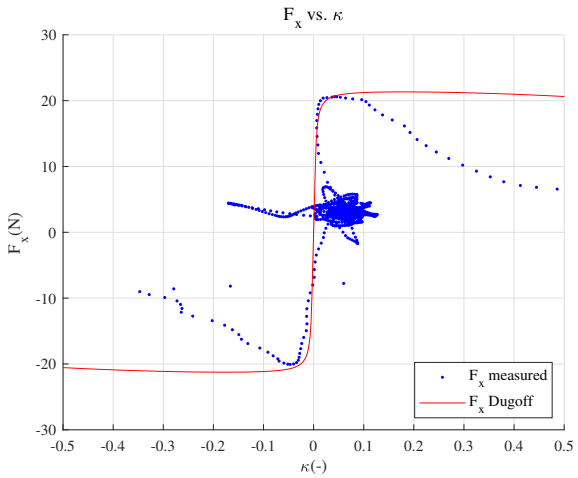

Fig. 16. Experiment 1(Lino): measured longitudinal traction force F_x vs measured slip coefficient κ with Dugoff model.

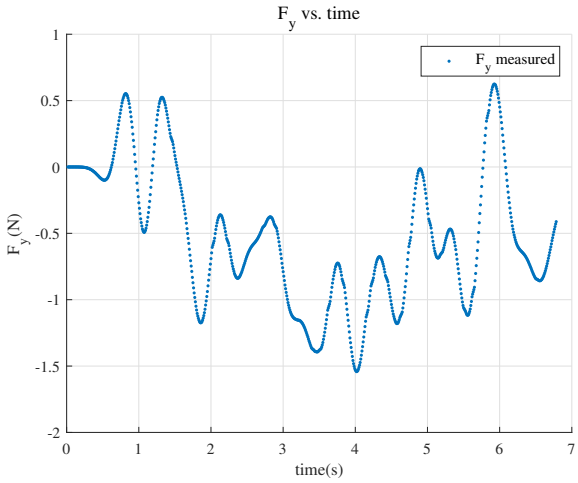

Fig. 17. Experiment 1 (Lino): measured lateral skid force F_y vs time.

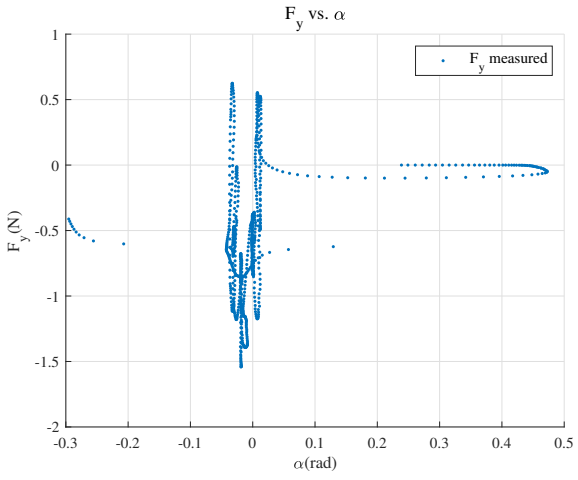

Fig. 18. Experiment 1 (Lino): measured lateral skid force F_y vs measured slip angle α.

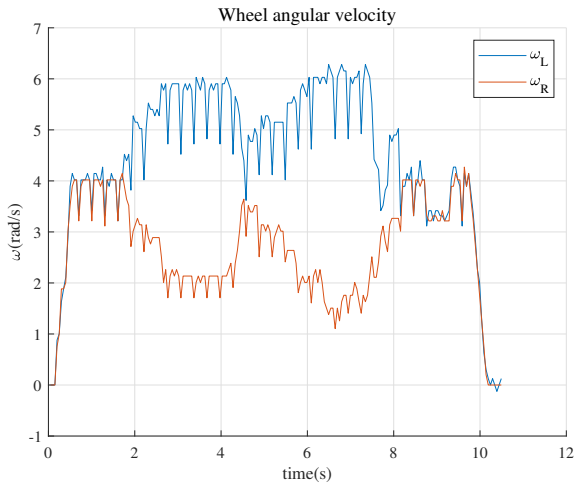

Fig. 19. Experiment 4 (Lino): Graphical representation of the angular velocities of the left- and right side wheels.

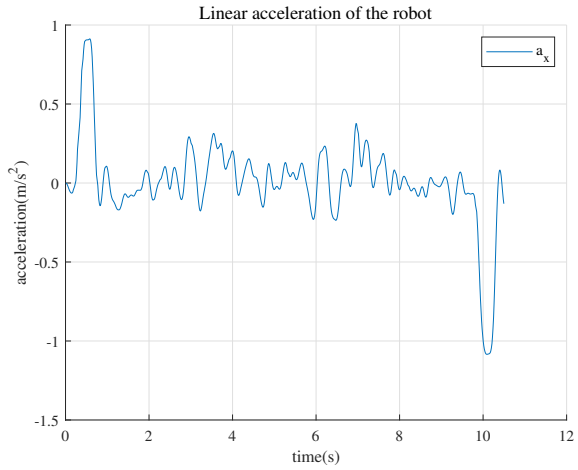

Fig. 20. Experiment 4 (Lino): Graphical representation of the linear acceleration of the Jackal robot.

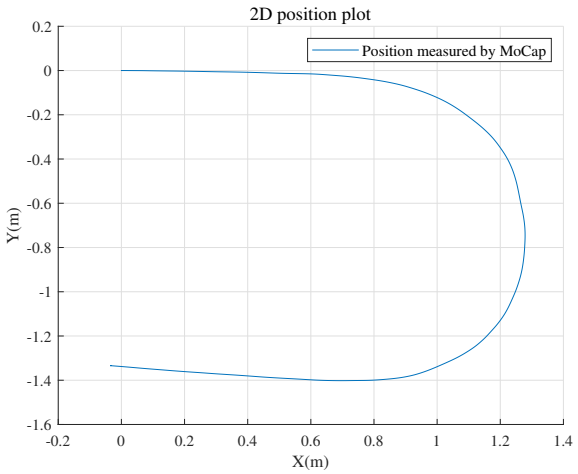

Fig. 21. Experiment 4 (Lino): Graphical representation of the 2D trajectory of the Jackal robot starting at (0,0).

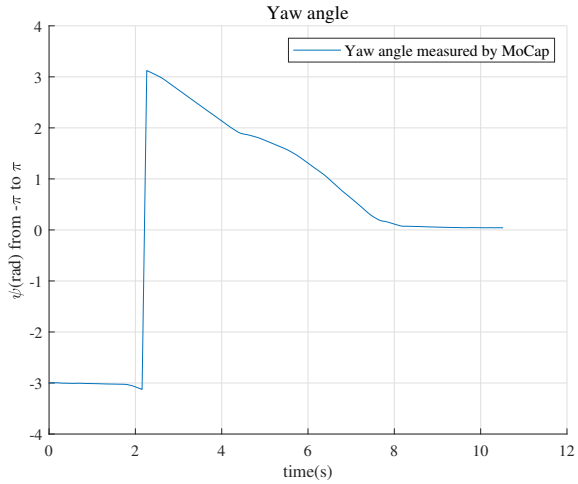

Fig. 22. Experiment 4 (Lino): Graphical representation of the yaw angle of the Jackal with respect to the global frame.

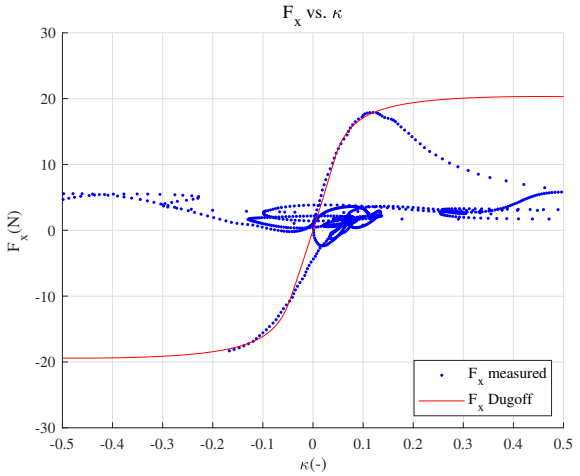

Fig. 25. Experiment 4 (Lino): measured linear traction force F_x vs measured slip coefficient κ with Dugoff model.

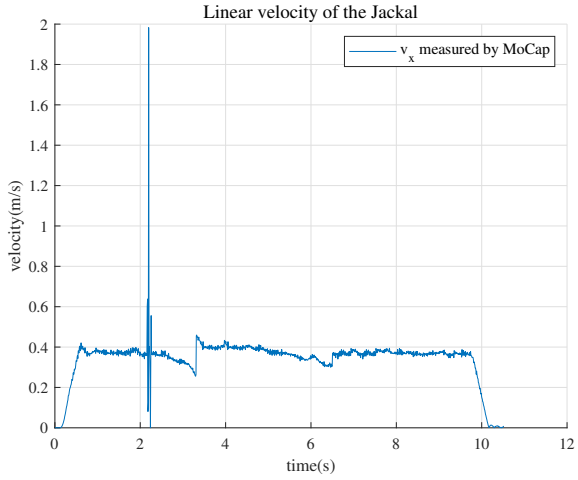

Fig. 23. Experiment 4 (Lino) : Graphical representation of the linear velocity of the Jackal in the local frame.

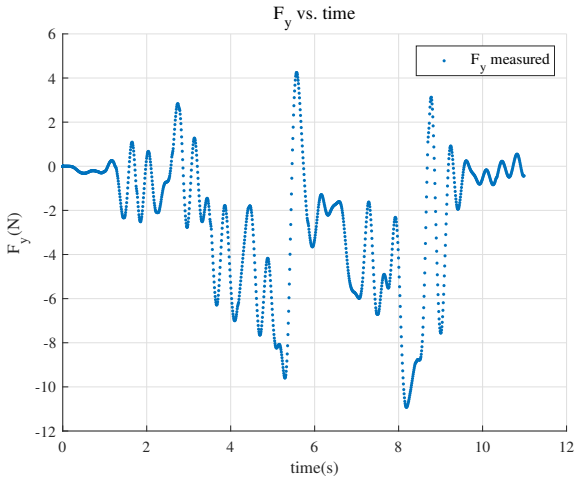

Fig. 26. Experiment 4 (Lino): measured lateral skid force F_y vs time.

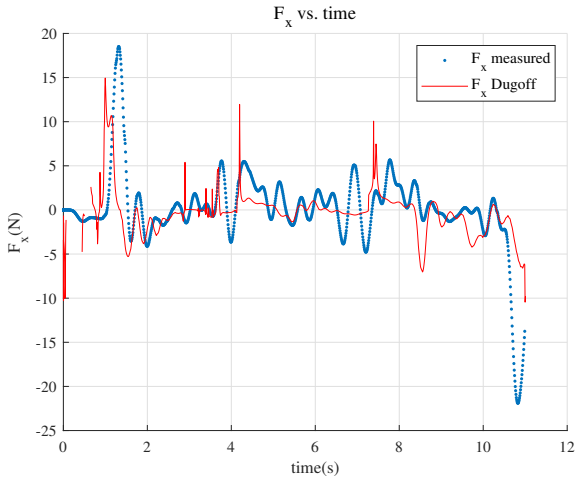

Fig. 24. Experiment 4 (Lino): Graphical representation of the measured linear traction force F_x vs time.

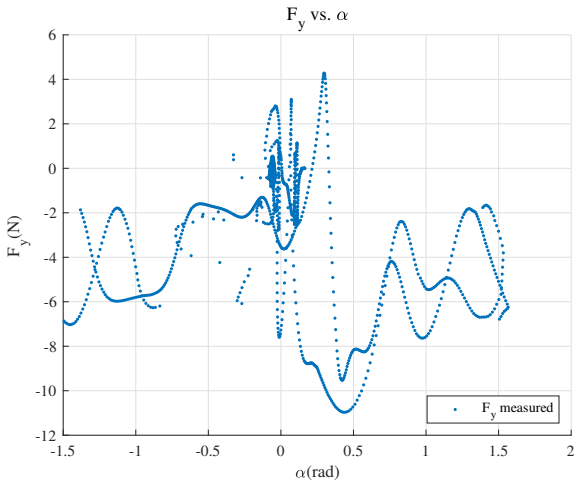

Fig. 27. Experiment 4 (Lino): measured lateral skid force F_y vs measured slip angle α.

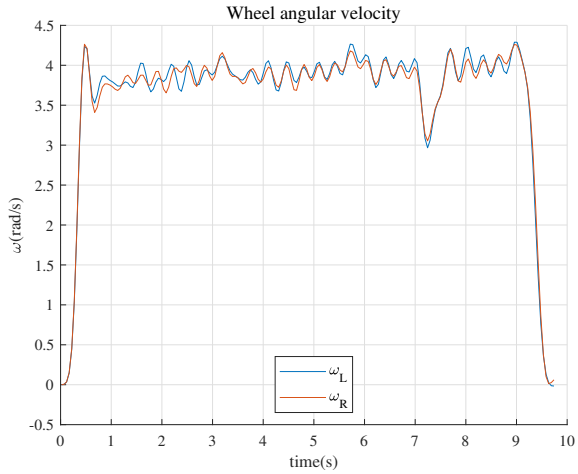

Fig. 28. Experiment 1 (Carpet): Graphical representation of the angular velocities of the left- and right side wheels.

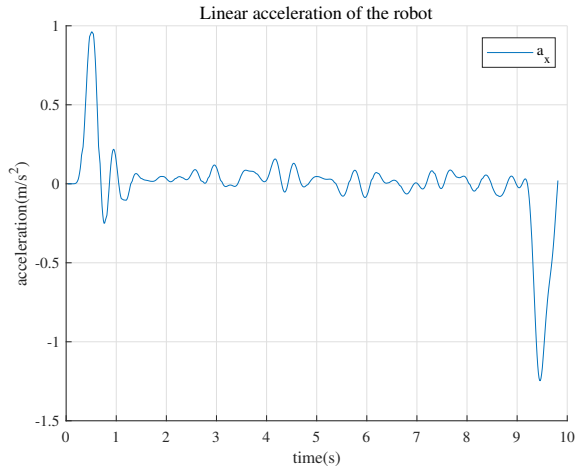

Fig. 29. Experiment 1 (Carpet): Graphical representation of the linear acceleration of the Jackal robot.

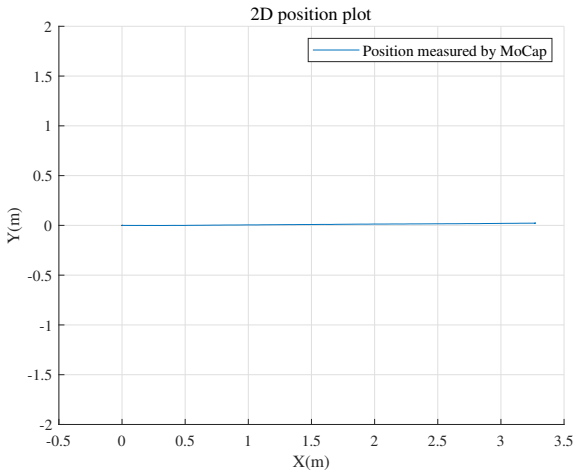

Fig. 30. Experiment 1 (Carpet): Graphical representation of the 2D trajectory of the Jackal robot starting at (0,0).

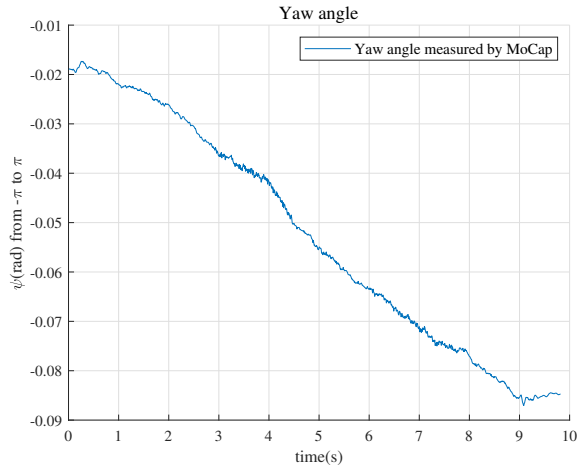

Fig. 31. Experiment 1 (Carpet): Graphical representation of the yaw angle of the Jackal with respect to the global frame.

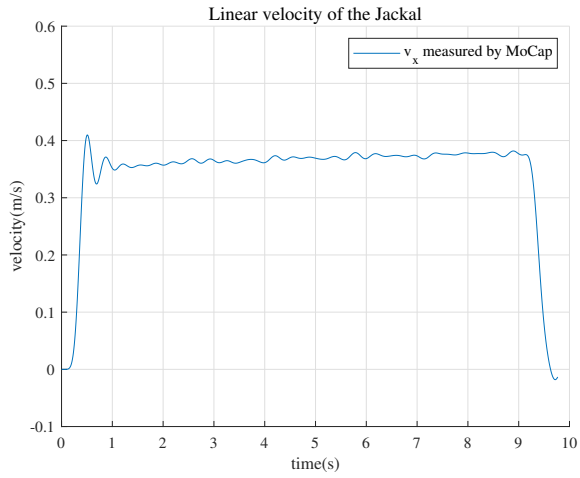

Fig. 32. Experiment 1 (Carpet): Graphical representation of the linear velocity of the Jackal in the local frame.

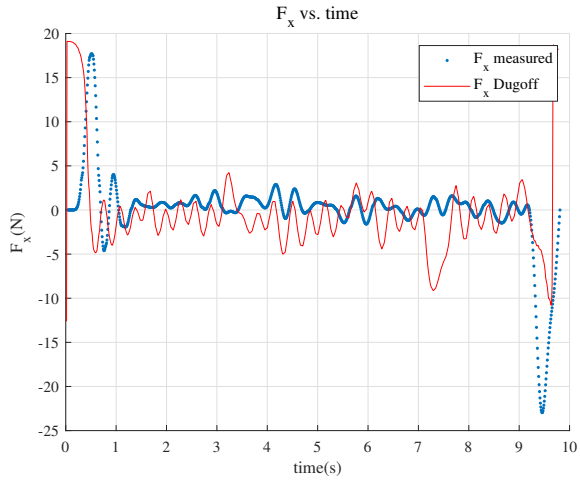

Fig. 33. Experiment 1 (Carpet): measured longitudinal traction force F_x vs time with Dugoff model.

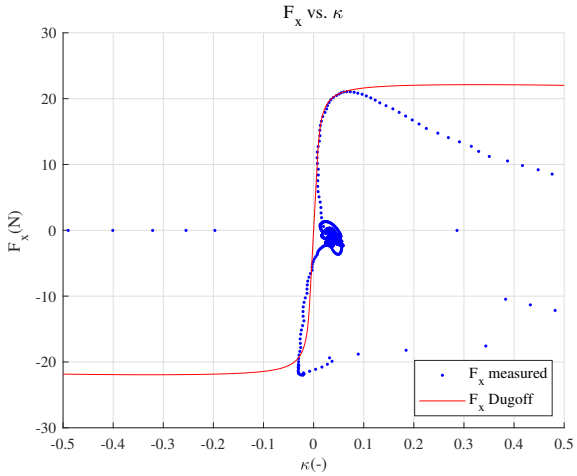

Fig. 34. Experiment 1 (Carpet): measured longitudinal traction force F_x vs measured slip coefficient κ with Dugoff model.

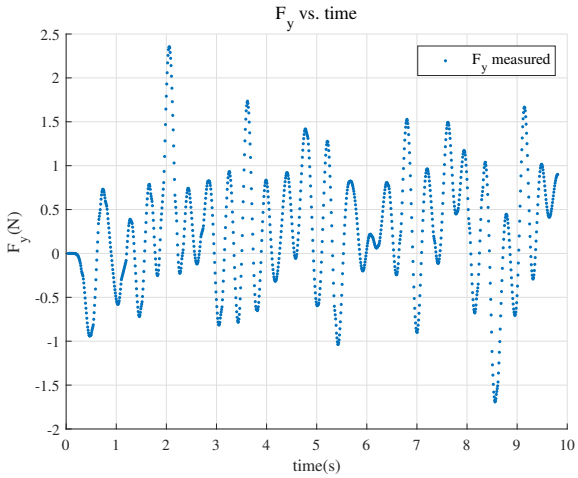

Fig. 35. Experiment 1 (Carpet): measured lateral skid force F_y vs time.

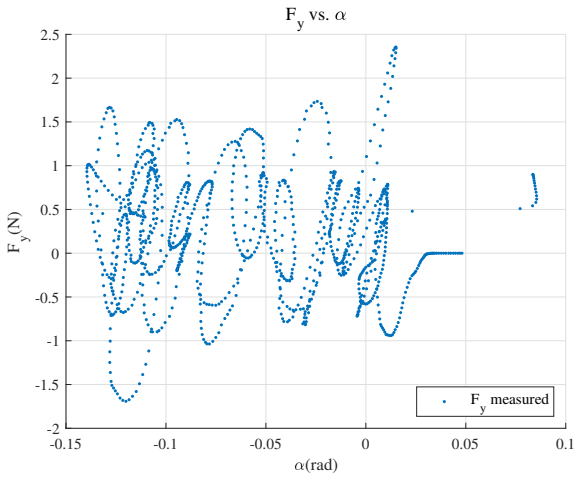

Fig. 36. Experiment 1 (Carpet): measured lateral skid force F_y vs measured slip angle α.

Appendix C - Structural parameters robot

TABLE IV
STRUCTURAL PARAMETERS OF THE JACKAL

Parameter	**Symbol**	**Value**	**Units**
Mass	m	16.532	kg
Wheel mass	m_{wheel}	0.477	kg
Wheel radius	r	90	mm
Wheel width	t	40	mm
Wheelbase	$l_{\text{wheelbase}}$	0.262	m
Moment of inertia wheel, xx	$I_{xx,wheel}$	0.0013	kgm^2
Moment of inertia wheel, yy	$I_{yy,wheel}$	0.0024	kgm^2
Moment of inertia wheel, zz	$I_{zz,wheel}$	0.0013	kgm^2
Chassis length	l_{chassis}	420	mm
Chassis width	W	310	mm
Chassis heigth	H	420	mm
Moment of inertia chassis, xx	$I_{xx,chassis}$	0.3136	kgm^2
Moment of inertia chassis, yy	$I_{yy,chassis}$	0.0.3922	kgm^2
Moment of inertia chassis, zz	$I_{zz,chassis}$	0.4485	kgm^2
DC motor inductance	L_{motor}	0.22	mH
DC motor resistance	R_{motor}	0.5	Ω
Gearhead ratio	j	25.01	-
Gearhead efficiency	η	0.75	-